Invited Review

K-Space in the Clinic

Cynthia B. Paschal, PhD,[1,2]* and H. Douglas Morris, PhD[3]

Magnetic resonance imaging (MRI) sequences are characterized by both radio frequency (RF) pulses and time-varying gradient magnetic fields. The RF pulses manipulate the alignment of the resonant nuclei and thereby generate a measurable signal. The gradient fields spatially encode the signals so that those arising from one location in an excited slice of tissue may be distinguished from those arising in another location. These signals are collected and mapped into an array called k-space that represents the spatial frequency content of the imaged object. Spatial frequencies indicate how rapidly an image feature changes over a given distance. It is the action of the gradient fields that determines where in the k-space array each data point is located, with the order in which k-space points are acquired being described by the k-space trajectory. How signals are mapped into k-space determines much of the spatial, temporal, and contrast resolution of the resulting images and scan duration. The objective of this article is to provide an understanding of k-space as is needed to better understand basic research in MRI and to make well-informed decisions about clinical protocols. Four major classes of trajectories—echo planar imaging (EPI), standard (non-EPI) rectilinear, radial, and spiral—are explained. Parallel imaging techniques SMASH (simultaneous acquisition of spatial harmonics) and SENSE (sensitivity encoding) are also described.

Key Words: k-space; spatial frequency; trajectory; echo planar imaging; spiral; parallel imaging
J. Magn. Reson. Imaging 2004;19:145–159.
Published 2004 Wiley-Liss, Inc.†

MAGNETIC RESONANCE IMAGING (MRI) techniques are defined by a sequence of radio frequency (RF) pulses and time-varying gradient magnetic fields. Variations in RF pulses and gradient magnetic field waveforms lead to a multitude of MRI techniques and options within a given technique. Many of these variations have to do with how the signals are spatially encoded by the gradient magnetic fields, i.e., how information from tissue in one location is differentiated from that of tissue in another location. During scanning, these signals are written into an array called k-space. Then a reconstruction algorithm—most often the Fourier transform (FT)—is used to take the k-space information and convert it to an image. How signals are mapped into k-space can have a dramatic effect on the spatial, temporal, and contrast resolution of the resulting images and on scan duration. The objective of this article is to provide an understanding of k-space as is needed to better understand basic research in MRI and to make well-informed decisions about clinical protocols. Additional, very useful reviews of k-space have been published by Hennig (1) and Mezrich (2) and encompassed in a review by Duerk (3).

MRI is an extremely flexible modality allowing multidimensional imaging in any scan orientation with a variety of temporal, spatial, and contrast resolutions. Flexibility leads to complexity, so for the sake of simplicity in this article, some basic assumptions are made. First, it is assumed that the vertical direction of an image lies along the y axis and that the technique of phase encoding is used to localize signals along this axis. The horizontal direction is assumed to lie along the x axis, and readout or frequency encoding is assumed to localize signals along this axis. The corresponding coordinate axes in k-space will be called the k_y axis and the k_x axis. Second, this paper will focus only on two-dimensional imaging, although the principles described here extend directly to three-dimensional imaging. Finally, for simplicity, the fact that k-space and image space points are complex, meaning that they are represented by both real and imaginary numbers, will not be addressed.

SPATIAL ENCODING AND THE FT

Before launching into an exploration of k-space, it is important to review the basics of spatial encoding (4–9) and the FT (10). In MRI, passage of electric current through gradient coils leads to variations (gradients) in magnetic field as a function of position. The presence of these gradient magnetic fields causes tissue signals to have frequencies that are functions of position p, according to the fundamental relationship in MRI, the Larmor equation, given here in a simplified form:

$$frequency(p) = \gamma * B(p) = \gamma * (B_o + G * p)$$

[1]Department of Biomedical Engineering, Vanderbilt University School of Engineering, Nashville, Tennessee.
[2]Department of Radiology & Radiological Sciences, Vanderbilt University School of Medicine, Nashville, Tennessee.
[3]NIH Magnetic Resonance Facility, National Institute of Neurological Disorders and Stroke, Bethesda, Maryland.
*Address reprint requests to: C.B.P., Department of Radiology & Radiological Sciences, Vanderbilt University Medical Center, R-1321 MCN, 1161 21st Ave. South, Nashville, TN 37232-2675. E-mail: cynthia.paschal@vanderbilt.edu
Received July 7, 2003; Accepted October 17, 2003.
DOI 10.1002/jmri.10451
Published online in Wiley InterScience (www.interscience.wiley.com).

Published 2004 Wiley-Liss, Inc. †This article is a US Government work and, as such, is in the public domain in the United States of America.

where γ is the gyromagnetic ratio, a constant for a given nucleus; B is the magnetic field as a function of position (p); B_o is the static (main) magnetic field; and G is the gradient magnetic field applied along the position axis. In a completely homogeneous field (i.e., in the absence of encoding gradients and other sources of magnetic field variation such that $G = 0$), signals from all pixels have the same frequency and average phase. To have the same phase means that the magnetic moments of the nuclei point in the same direction, and thus their signals sum constructively. A collection of pixels producing signals of the same frequency and average phase is analogous to a chorus of altos singing in unison. Ignoring the spectral richness of the human voice and the stereo nature of auditory perception, in these circumstances it would not be possible for a listener at a distance to determine the location of the alto in the chorus who is singing the loudest, just as it would be impossible to tell what piece of tissue has the strongest MR signal in the absence of gradients. The trick in MRI is to change the magnetic field at each position in such a way that over the course of the entire scan, each unique location in the image experiences a unique combination of magnetic field variations. This leads to an unambiguous encoding of the MR signals. To continue the musical analogy, unambiguous encoding of chorister positions could be accomplished by instructing members of the all-alto chorus in the front row to start singing first, with the singers in the next row starting a measure later, and the third row yet a measure later. Then it would be possible to identify the relative loudness of each row based on the relative phase of each row of singers. If simultaneously the second singer in each row was asked to sing one key higher, the third to go up two keys, etc., then one could identify both the row and position within the row of the loudest singer. In the same way, tissues in MRI are encoded by the gradients to "sing" with phases and frequencies that are a unique function of position.

MRI signals, like sound, can be represented in two different and equivalent ways, each as functions of one of two related variables. Such pairs of variables include time and frequency for sound and spatial frequency and space for MRI. To explore these dual representations, the musical analogy is continued. When listening to singing or other sounds, the ear responds to oscillations in air pressure that occur over time. For example, when three piano keys are struck simultaneously (Fig. 1a), the vibrating piano strings make the surrounding air oscillate. The sinusoidal pressure waves generated by the three vibrating strings combine together into a more complex sound wave, as illustrated by Fig. 1b. It is this variation in air pressure as a function of time that makes the tympanic membrane and in turn specific regions of the basilar membrane of the cochlea oscillate maximally (Fig. 1c). The tonotopic mapping of the cochlea then allows the auditory system to separate the composite sound into sounds of different frequencies. The perceived sound is then loudness as a function of frequency or piano key, as in Fig. 1d. In other words, what is carried by the auditory nerve to the brain is tonal or frequency information, not the actual temporal oscillations in acoustic pressure. Both representations—sound intensity as a function of time and sound intensity as a function of frequency—equally demonstrate the same event and are related by an FT, which in the case of hearing is naturally performed by the cochlea. The FT is simply a mathematical tool that translates the expression of information in one domain, such as sound intensity as a function of time, into a related expression in another domain, such as sound intensity as a function of frequency. The FT is a loss-less transformation, and thus the expressions in each domain have the same information content. It is the representation of that content that differs between the two domains.

In an analogous way, an MR scanner records voltage oscillations in a receive coil that occur over time and represent the combination of signals of many different frequencies (positions). Then the FT performed by the MR scanner separates the composite signal into its constituent frequencies. More specifically, the FT translates receive coil voltage as a function of time-dependent *spatial frequency* coordinates k_x and k_y in the k-space domain into image intensity as a function of *spatial position* coordinates x and y in the image domain. Again, both representations—receive coil voltage as a function of spatial frequency and image intensity as a function of spatial position—equally characterize the same information and are related by an FT.

The magnitude of each point in k-space indicates how much a particular spatial frequency is represented in the imaged object. The phase of each point in k-space, which is embedded in the complex real and imaginary values, indicates how the given spatial frequency wave is positioned in image space (e.g., peak at the center, valley at the center, etc.).

K-SPACE

Just as the images we view in MR are two-dimensional arrays or matrices of intensities, the receive coil voltages we collect from the scanners are stored in two-dimensional k-space arrays. Examples of an image and the k-space array from which the image was calculated are shown in Fig. 2. The k-space location (k_x, k_y) to which the data from any one sampling point of any one repetition belong is governed by the accumulated effect of gradient events along the corresponding axis occurring after the excitation pulse up to the time at which that data sample is collected. Mathematically, the coordinates are given by

$$k_x(t') = \int_0^{t'} \gamma G_x(t)\,dt \quad \text{and} \quad k_y(t') = \int_0^{t'} \gamma G_y(t)\,dt \quad (1)$$

where γ is the gyromagnetic ratio, $G(t)$ is the strength of the gradient as a function of time, and t' is the time at which a data sample is collected. The details of the equations are not important to this discussion. What is important follows as take-home point (THP) 1: the net strength and duration of the gradient events govern how far and in what direction from the origin of k-space ($k_x = 0$, $k_y = 0$) a data point belongs. The greater the net

15222586, 2004, 2, Downloaded from https://onlinelibrary.wiley.com/doi/10.1002/jmri.10451 by Cochrane Chile, Wiley Online Library on [17/08/2023]. See the Terms and Conditions (https://onlinelibrary.wiley.com/terms-and-conditions) on Wiley Online Library for rules of use; OA articles are governed by the applicable Creative Commons License

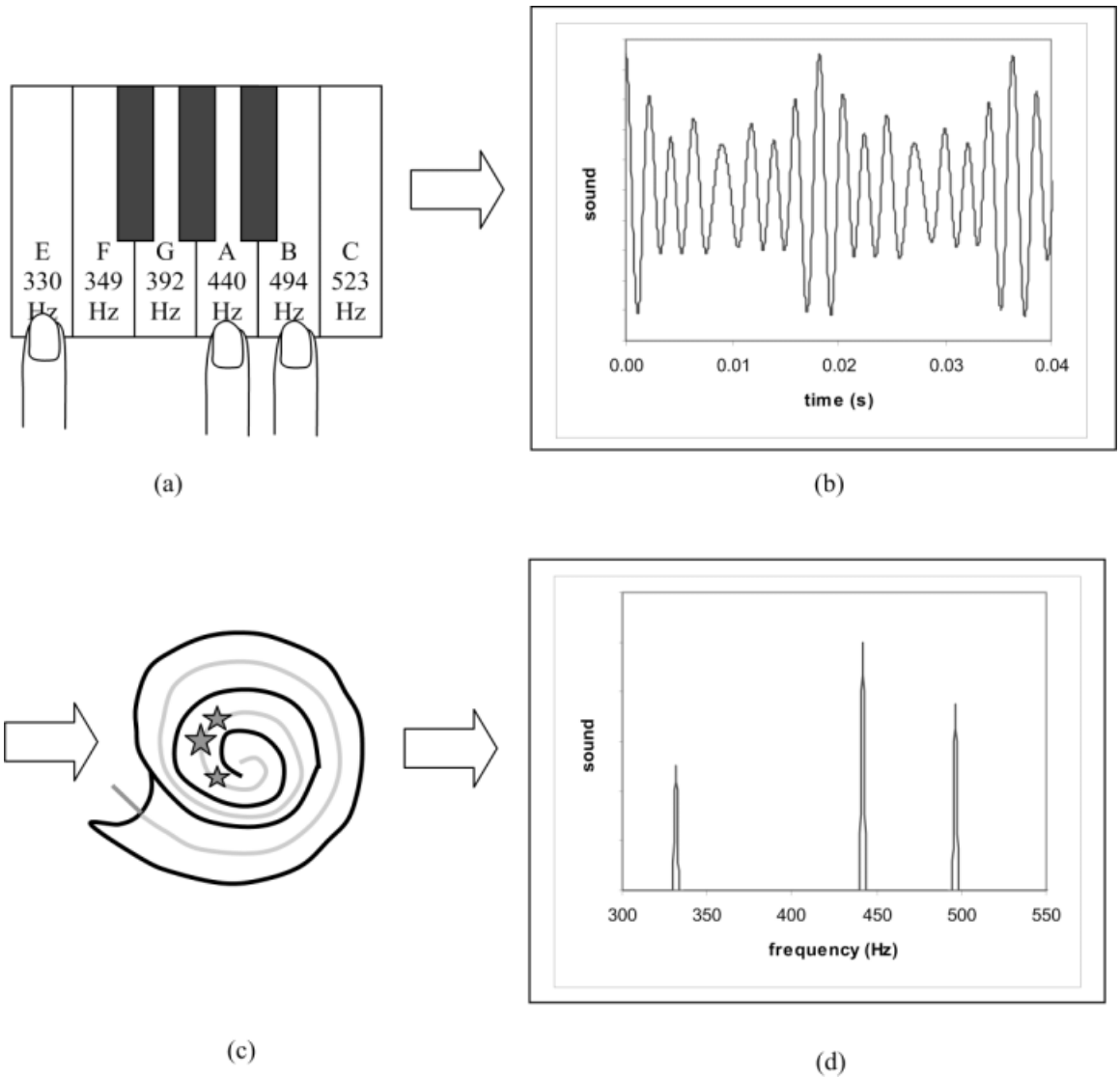

Figure 1. Sound is produced as oscillations in air as a function of time and perceived as tones of specific frequencies. If three piano keys are struck (**a**), the vibration of the strings causes the air and thus the tympanic membrane of the ear to oscillate with time. If we measure these oscillations, they might look like the graph in panel **b**. These sound waves produce an oscillation within the basilar membrane in the cochlea (**c**) where specific regions of the membrane (indicated by stars) respond maximally to the principal frequencies of the sound burst. The tonotopic mapping of the cochlea allows the brain to perceive the relative loudness of each specific frequency (or piano key), as shown in the spectrum (**d**). Both graphs b and d represent the sound produced by the piano and are related by the FT. The cochlea performs a natural FT. In an analogous way, the gradients of an MR scanner make tissues at different keys (locations) resonate at different frequencies, giving off a time signal measured by the receive coil that might look like the graph in panel b. A computer, rather than a cochlea, performs the FT to reveal an image of the relative signal strength of each key (tissue location), analogous to the graph in d.

strength of the gradient pulse and/or the longer a gradient is on with one polarity or sign, the farther from the k-space origin the data belong. Mathematically, as shown above, it is the integral or summation of the x gradient events that determines the k_x location of a data point, and similarly for the y gradient and k_y. In Fig. 3, the relationship between typical pulse sequence events and location in k-space is shown.

In addition to gradient events, a 180° RF pulse, such as is used in spin echo and some other pulse sequences, can change the k_x, k_y location of a data point in k-space. Such an RF pulse causes a jump to a new k_x, k_y location that is opposite the k_x, k_y location just prior to the 180° pulse.

While the action of gradients causes continuous change of the k_x and k_y coordinates, the MR signal is sampled at discrete times as is necessary for digital computer processing of the data. Recall that unambiguous encoding of tissue signals requires changes in the magnetic field at each spatial position in such a way that over the course of the entire scan, each unique location in the image experiences a unique combination of magnetic field variations. To successfully capture these unique combinations of field variations, the MR

15222586, 2004, 2, Downloaded from https://onlinelibrary.wiley.com/doi/10.1002/jmri.10451 by Cochrane Chile, Wiley Online Library on [17/08/2023]. See the Terms and Conditions (https://onlinelibrary.wiley.com/terms-and-conditions) on Wiley Online Library for rules of use; OA articles are governed by the applicable Creative Commons License

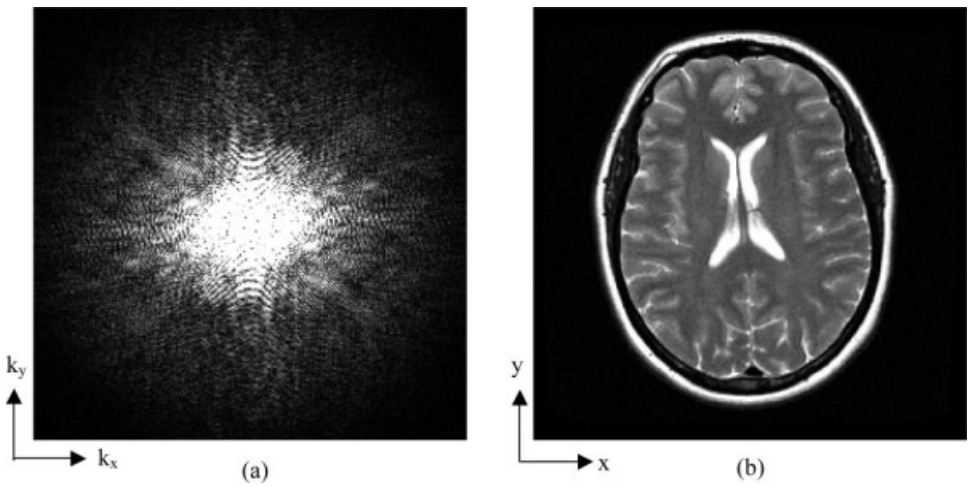

Figure 2. Raw data in k-space array (**a**) and corresponding image data in image space (**b**). In both cases, the magnitude of the data is presented.

signal must be sampled at appropriately frequent time intervals. Otherwise, if the sampling is too coarse in time, encoding is ambiguous and aliasing results in the image. The appropriate sampling frequency is defined by the Nyquist frequency (10,11).

The number of points collected along any axis in k-space is typically a power of 2 (e.g., 64, 128, or 256). This is because MR scanners use a rapid, efficient version of the discrete FT, the so-called fast FT, or FFT, that requires 2^n points (10).

The coordinates of k-space are spatial frequencies with units of reciprocal distance, such as millimeter^{-1}. Spatial frequency describes the rate at which image features change as a function of position. The MR image signals from a large, fairly uniform object, such as a healthy liver, essentially do not change over a long range of spatial positions. So, the liver is said to produce an abundance of low-spatial-frequency signals. However, when the edge of the liver is encountered, image signal changes rapidly as a function of position. Edges are represented by high spatial frequencies. Low-amplitude and/or short-duration gradient events encode low-spatial-frequency information such as the general shape of the liver; these data are mapped to the center of k-space. Conversely, high-amplitude and/or long-duration gradient events encode high-spatial-frequency information such as the edges of the liver or a blood vessel; this information is mapped to the periphery of k-space. This is take-home point 2. This arrangement is illustrated in Fig. 4 with a rectilinear k-space sampling grid highlighting the relations between Δk_x and Δx, and similarly for Δk_y and Δy. An image reconstructed from the low-spatial-frequency data mapped to the center of k-space is of low resolution (Fig. 5a), while an image reconstructed from only the data in the periphery of k-space reveals a faint image of only the high-spatial-frequency details of the image—namely, the edges (Fig. 5b).

Beginning with the low-spatial-frequency information at the center of k-space and adding progressively more peripheral data in the reconstruction improves the spatial resolution of the image (Fig. 6a–d). Thus, we come to take-home point 3: the farther our data collection extends from the origin of k-space, the better the

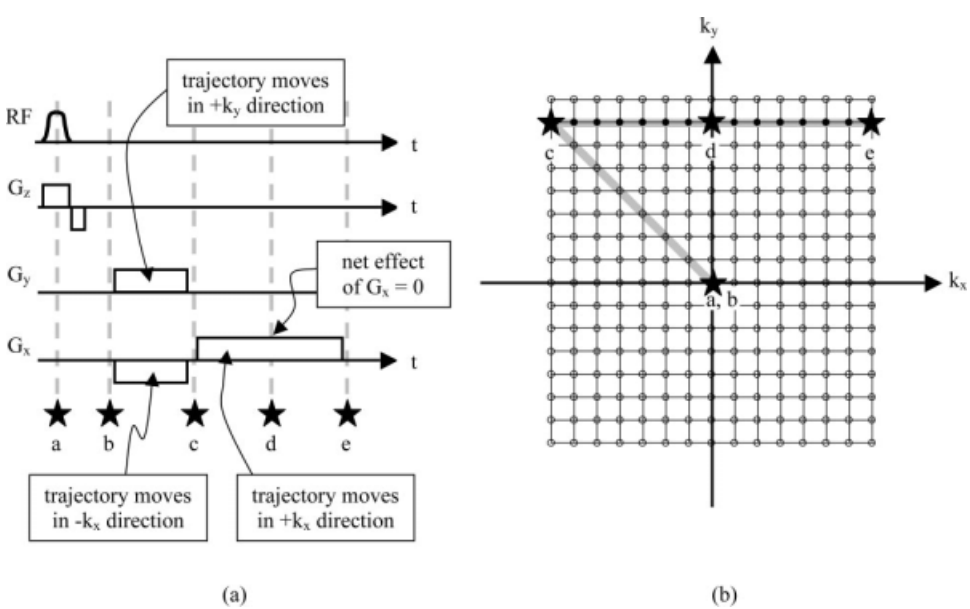

Figure 3. Gradient echo pulse sequence (**a**) and corresponding k-space trajectory (**b**). Each x and y gradient event leads to a change in k-space position, according to the time integral of the gradient. Lettered stars indicate time points with correspondence between the pulse sequence (a) and k-space trajectory (b). Filled-in dots on the k-space trajectory indicate data points collected in this one repetition of the pulse sequence.

15222586, 2004, 2, Downloaded from https://onlinelibrary.wiley.com/doi/10.1002/jmri.10451 by Cochrane Chile, Wiley Online Library on [17/08/2023]. See the Terms and Conditions (https://onlinelibrary.wiley.com/terms-and-conditions) on Wiley Online Library for rules of use; OA articles are governed by the applicable Creative Commons License

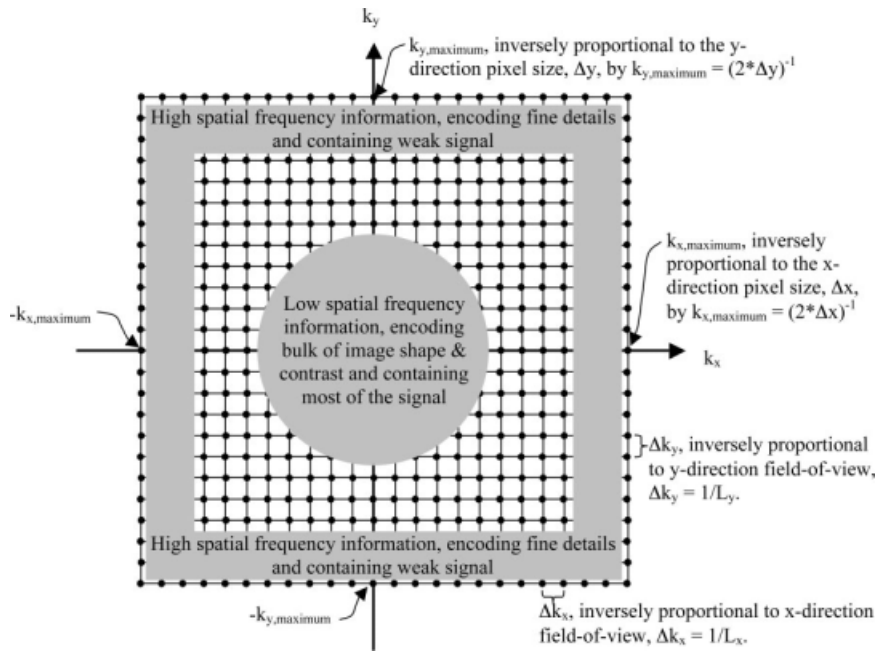

Figure 4. General features of k-space.

nominal spatial resolution of our image. Adding the high-spatial-frequency information sharpens the image but does not change contrast or the general shapes in the image. This brings us to take-home point 4: most image information, including contrast and general shape, is contained in the low-spatial-frequency data mapped to the center of k-space. This has important implications regarding image contrast and effective echo time for certain pulse sequences.

Application of gradient magnetic fields dephases or reduces the total strength of the MR signal. Considering the readout gradient in particular, when the dephasing effects of a negative gradient event are completely reversed by a positive gradient event, a gradient echo

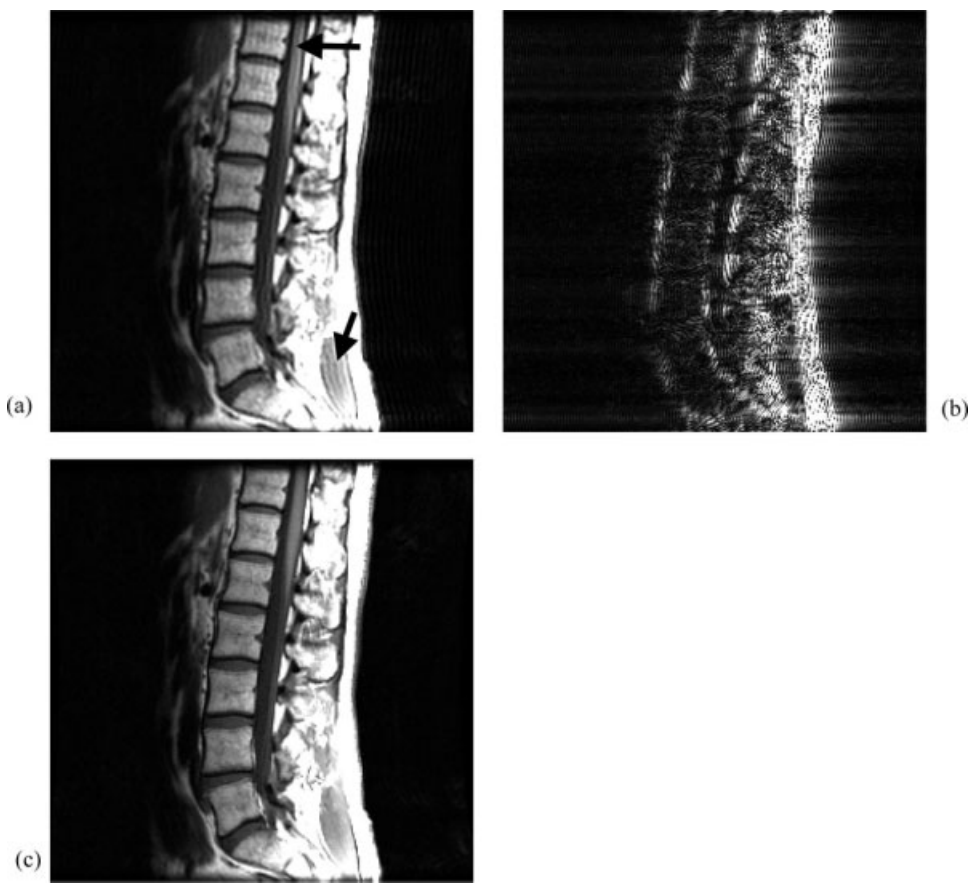

Figure 5. a: Using only the central 128 × 128 low-spatial-frequency data points in a k-space array and replacing the peripheral data with zeros, a somewhat low-resolution image of the lumbar spine is produced. **b:** Using instead the peripheral high-spatial-frequency k-space data and zeroing out the central 128 × 128 data points produces an image of only the high-spatial-frequency details of the image—namely, the edges. The image reconstructed from the full 256 × 256 k-space array is provided for reference (**c**). In comparing images a and c, note that the truncation or omission of the high-spatial-frequency information in panel a results in ringing (Gibb's ringing or truncation artifact) near edges (arrows). Such ringing in images of the cervical spine can be misinterpreted as a syrinx (12).

15222586, 2004, 2, Downloaded from https://onlinelibrary.wiley.com/doi/10.1002/jmri.10451 by Cochrane Chile, Wiley Online Library on [17/08/2023]. See the Terms and Conditions (https://onlinelibrary.wiley.com/terms-and-conditions) on Wiley Online Library for rules of use; OA articles are governed by the applicable Creative Commons License

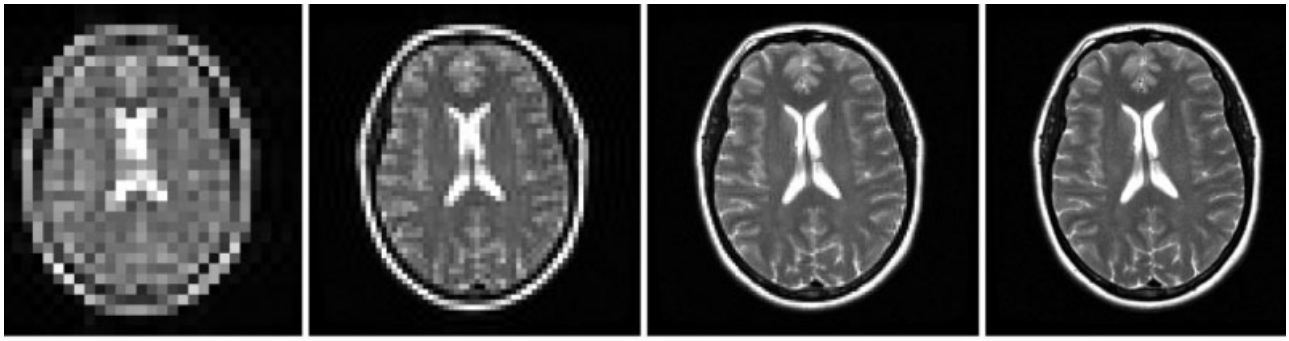

Figure 6. Beginning with the low-spatial-frequency information at the center of k-space and adding progressively more peripheral high-spatial-frequency data in the reconstruction improves the spatial resolution of the image (THP 3). **a:** 32 × 32 points. **b:** 64 × 64 points. **c:** 128 × 128 points. **d:** 256 × 256 points. Note that the general contrast and shape are the same in all four images, illustrating the fact that the center of k-space encodes the bulk of the image information (THP 4), though the increasing resolution reduces the loss of apparent contrast due to partial averaging of large voxels.

occurs. This echo is mapped to the center of the k_x axis ($k_x = 0$) since the net effect of the x gradient is zero. This can be visualized by noting that the net area of the x gradient events is zero at the time the $k_x = 0$ data point is collected (see Fig. 3).

The nominal echo time, TE, is equal to the time within an excitation that the data point at the k-space origin ($k_x = 0$, $k_y = 0$) is acquired. Recalling that most image information is contained in the low-spatial-frequency data mapped to the center of k-space (THP 4), we see that the TE has a significant impact on image contrast. It is important to note that the time at which other adjacent low-spatial-frequency data is acquired also affects image contrast. For the most basic scans in which one line of k-space data is acquired in each repetition (e.g., standard spin echo and gradient echo scans), the $k_x = 0$ point of each k_y line is acquired at the same time after the excitation and the points on either side of $k_x = 0$ are acquired symmetrically about TE over a short time window. In such simple rectilinear scans, TE (along with TR) is a concise and thorough description of the impact of data collection timing on contrast. With other scanning techniques, data for different lines may be collected at different delays after the excitation (e.g., multiecho scanning), the time window around TE over which data is collected may be much longer (e.g., echo planar imaging (EPI)), or the collection of data may not be temporally symmetric around the TE (e.g., spiral scanning). In these cases, a single TE value, while definable, does not completely describe the impact of data collection timing on contrast.

It is useful to know a few simple relations regarding k-space and the spatial (image) domain. Related to THP 3, the extent of k-space coverage along one spatial frequency axis (e.g., $k_{x,maximum}$; see Fig. 4) is inversely proportional to the pixel dimension (Δx) along the corresponding spatial axis (specifically, $k_{x,maximum} = (2*\Delta x)^{-1}$). The separation between adjacent points in k-space (Δk) is inversely proportional to the field of view (L) along the corresponding spatial axis (e.g., $\Delta k_y = 1/L_y$). When a pulse sequence is designed such that the k-space points are spaced as described, tissue signals across the field of view are uniquely encoded and no aliasing of these signals occurs. Note that the pixel dimension, field of view, and number of pixels along each dimension are not necessarily the same. Finally, it is important to know that in the ideal k-space, data are symmetric about the origin, meaning that the first and third quadrants of a k-space array are mirror images of each other, as are the second and fourth. This arises from the fact that k-space data are representations of an image as a collection of cosine and sine waves of different frequencies and that such waves are symmetric ($\cos(k_x) = \cos(-k_x)$) and antisymmetric ($\sin(k_x) = -\sin(-k_x)$). In practice, this perfect symmetry is rarely achieved. Acquiring both halves of the k-space data increases the signal-to-noise ratio (SNR) by $\sim \sqrt{2}$.

K-SPACE TRAJECTORIES

There are many different ways to collect the data necessary for an image. This is called filling k-space, and the order in which (k_x, k_y) points are acquired is described by the k-space trajectory, or trajectory for short. There are four major classes of trajectories: standard non-EP rectilinear, EP, radial, and spiral. Within these classes of trajectories, there are often variations related to the timing of data acquisition related to changes such as passage of a contrast agent bolus or cardiac cycle motion. These different trajectories with many of their major variations are summarized in Table 1 and are discussed in the following sections.

Non-EPI Rectilinear Trajectories

Currently, most MRI techniques use a line-by-line rectilinear trajectory in which a line of data, comprised of all the k_x values for a fixed k_y value, is acquired after one excitation. Then, after the repetition time TR, another excitation occurs and another line is acquired. Thus, scan time is equal to #k_y lines * TR * (number of signals averaged or NSA or NEX). Such a rectilinear trajectory can be used with spin echo (SE), gradient echo (GE), inversion recovery (IR), and a number of other pulse sequences. There are a number of variations on rectilinear scanning as noted in Table 1; these were devel-

15222586, 2004, 2, Downloaded from https://onlinelibrary.wiley.com/doi/10.1002/jmri.10451 by Cochrane Chile, Wiley Online Library on [17/08/2023]. See the Terms and Conditions (https://onlinelibrary.wiley.com/terms-and-conditions) on Wiley Online Library for rules of use; OA articles are governed by the applicable Creative Commons License

Table 1
Summary of k-Space Filling Strategies*

Trajectory	Major options	Comments	Application
Standard (non-EPI) rectilinear	Sequential	Acquire each k_y-line in a separate readout, in order from top to bottom of k-space.	For standard imaging applications in which relative contrast is constant from excitation to excitation (i.e., steady state imaging).
	Centric	Acquire each k_y-line in a separate readout, starting at the center line of k-space ($k_y = 0$) and alternating up and down on successive excitations.	For applications in which intent is to have initial relative contrast dominate the image contrast such as after a preparatory RF pulse or contrast agent injection (non-steady state imaging).
	Reverse centric	Acquire each k_y-line in a separate readout, starting with the outer lines of k-space ($k_y = +k_{y,\ maximum}$ and $-k_{y,\ maximum}$) and working inward from either edge in successive excitations.	For applications in which intent is to have final relative contrast dominate the image contrast such as after a preparatory RF pulse (non-steady state imaging).
	View-sharing	Acquire incomplete sets of k_y lines for different cine phase images. Then, share k_y lines from temporally adjacent acquisitions to complete the k-space matrix for each cine phase image.	For cine applications in which short total scan times and high temporal resolution with good spatial resolution are needed. Temporal blurring results.
	Keyhole	Acquire a complete k-space matrix, one line at a time, typically in order from top to bottom of k-space. Then, periodically update the central lines, reconstructing them with the older peripheral lines.	For imaging dynamic events in which producing multiple images with high temporal resolution is more important than highly accurate spatial resolution.
	Fast spin echo/turbo spin echo	Acquire multiple lines of k-space data per excitation with each line acquired after a new ~180° pulse generates an echo.	For reducing total scan time for long TR scans. Provides a mixture of T2 contrast since multiple TE's are used.
	Half-Fourier or partial Fourier	Acquire the lines to fill in a bit more than the upper half of k-space. Then capitalize on the symmetry of k-space to replace the missing data with a reasonable estimate.	For situations in which reducing the scan time by a factor of almost 2 is worth the associated loss of SNR in proportion to almost (1/2).
	Zero padding/Interpolation	Acquire the central k_y lines (N_{acq}, typically at least half the desired matrix size, $N_{desired}$) and replace the missing data with zeros. This "zero padding" in k-space is equivalent to interpolating a low resolution image to make a higher resolution image.	For situations in which reducing the scan time by a factor of $N_{acq}/N_{desired}$ is worth the associated loss of SNR in proportion to the square root of that same factor. This commonly occurs when a 256×128 matrix is used for acquisition but a 256×256 image is displayed.
EPI	Blipped—single shot	Traverse all of k-space, covering a rectilinear grid, starting in one corner, sweeping across the k_x axis for a given k_y value, then jumping ("blipping") to the next k_y value and sweeping back across the k_x axis. Another blip to the next k_y value follows and so on until all of k-space is traversed. Since the acquired data points fill the grid of a k-space matrix, no regridding (interpolation) of data points is need for blipped EPI.	For applications requiring very fast acquisitions. Especially good for functional MRI (fMRI) studies due to high speed and sensitivity to BOLD effect. Distortions and T2* dependent signal loss typically prohibit the acquisition of a high resolution image.
	Blipped—multishot	Sparsely traverse all of k-space, starting in one corner, sweeping across the k_x axis for a given k_y value, then jumping ("blipping") to a different k_y value and sweeping back across the k_x axis. Another blip to another k_y value follows and so on until a fraction of k-space equal to 1/(#shots) is filled. Data from more than one excitation, each with a unique k-space trajectory are interleaved and then Fourier transformed to make one image.	For applications requiring very fast acquisitions but not as fast as single shot EPI. May also be used to fill a larger k-space matrix and thus obtain better spatial resolution than possible with single shot EPI. Since time spent acquiring data is shorter than with single shot EPI, distortions and signal loss are less severe.
Radial	Projection reconstruction	Traverse one radial line of k-space per excitation, with the lines from successive excitations filling in k-space like the spokes of a bicycle wheel.	For applications requiring extremely short TE such as imaging short T2* tissues like lung parenchyma or tissues in the vicinity of a field distortion. Since the periphery of k-space is sparsely sampled, fine details in the image are not well resolved. Heavy sampling of the center of k-space reduces motion artifacts and improves SNR.

15222586, 2004, 2, Downloaded from https://onlinelibrary.wiley.com/doi/10.1002/jmri.10451 by Cochrane Chile, Wiley Online Library on [17/08/2023]. See the Terms and Conditions (https://onlinelibrary.wiley.com/terms-and-conditions) on Wiley Online Library for rules of use; OA articles are governed by the applicable Creative Commons License

Table 1
(Continued)

Trajectory	Major options	Comments	Application
	PROPELLER (13)	Traverses k-space radially in groups parallel and centered about the k(0,0) point. The groups, also known as "blades" are rotated about the k(0,0) point of k-space like unto a rotating propeller.	Advantages include a more rapid coverage of the blade in k-space for a scan duration similar to EPI speeds and a high coverage of the outer portions of k-space. The technique maintains the robustness of radial sampling to bulk motion of the object but without the associated blurring due to reduced higher k-space acquisitions.
Spiral	Spiral out	Traverse all of k-space in a spiral pattern, starting at the center of k-space and spiraling outward.	For applications requiring single shot acquisition and the shortest possible nominal TE. (Interleaved multi-shot versions also used.) The symmetry of k-space coverage and the early sampling of the center of k-space relative to the excitation reduce motion and field-dependent distortions although blurring is evident.
		If a 2D FT is to be used for image reconstruction, spiral data must be regridded (interpolated to fill a grid) since the acquired data points do not fall on a grid in k-space.	
	Spiral in	Traverse all of k-space in a spiral pattern, starting at the periphery of k-space and spiraling inward.	For applications requiring single shot (extremely fast) acquisition with high SNR for the peripheral k-space data and a longer nominal TE. May be combined with spiral out data for BOLD sensitivity with less signal drop out.
	Multiple spirals	Sparsely traverse all of k-space with multiple, interleaved spirals, each acquired after a separate acquisition. Data from each spiral are interleaved and then reconstructed to make one image.	For applications requiring very fast acquisitions but not as fast as single shot spiral imaging. May also be used to fill k-space more densely thus obtain better spatial resolution and SNR.
Parallel imaging	SMASH	Uses specific receiver coil geometries to create additional k-space information without added scans.	For applications requiring reduced imaging time that can withstand the reduction in SNR, typically dynamic events like cardiac imaging, perfusion imaging, etc.
	SENSE	Uses receiver coil array sensitivity maps to compute missing data from an undersampled scan.	For applications requiring reduced imaging time that can withstand the reduction in SNR, typically dynamic events like cardiac imaging, perfusion imaging, etc.

*This table summarizes some of the most common methods for filling k-space, organized according to trajectory.

oped for situations in which some aspect of the imaged object changes over time, such as contrast or position, or in which reducing scan time is critical.

These non-EPI trajectories have the advantage that data acquisition time within any one excitation is short relative to the signal decay constant T2* and relative to the time it takes for chemical shift, magnetic susceptibility, and other field distortion artifacts (14–19) to evolve to an easily noticed level. Such artifacts, typically seen as distortions and blurring, are most readily seen across the image space dimension corresponding to the k-space axis that was most slowly traversed, which in non-EPI rectilinear trajectories is the readout (x) direction. This is take-home point 5. Even so, the time it takes to traverse the readout axis once is very short, on the order of a few milliseconds. Consequently, artifacts related to long-duration trajectories are minimized in non-EPI rectilinear scanning. Since phase encoding always occurs at the same time point within each repetition, with no evolution of signal across multiple repetitions for most sequences, time is in essence frozen for traversal of the k_y axis, and thus evolution artifacts are not seen in the y direction. Of course, many other artifacts arise if there are signal changes from k_y line to k_y line, most notably motion artifacts such as ghosting and blurring (20–23).

EP Trajectories

EP trajectories sweep back and forth across k-space very rapidly such that the entire k-space matrix, or a large portion of it, is filled in one execution of the pulse sequence. The trajectory typically begins in one corner of k-space and ends in the diagonally opposite corner. If the entire k-space matrix is filled in one execution of the pulse sequence, then it is termed a single-shot acquisition. Scan time is then only the echo time TE plus the time it takes to finish the second half of the data sampling, with the first half of the data collected prior to TE. If instead more than one execution of the pulse sequence is required to collect all the desired k-space data, then the scan is a multishot acquisition and scan time is TR times the number of shots (executions). The k-space trajectory for a typical EPI technique is shown in Fig. 7a. Note that the acquired data points for this blipped trajectory lie on a grid, which conveniently suits the application of an FT to reconstruct the image. Less commonly used EPI trajectories are sinusoidal (24), trapezoidal, and triangular (25), which utilize interpolation (regridding) or nonlinear data sampling to fit the data to a grid suitable for a two-dimensional FFT.

The attraction of EPI is its very short scan times. This, combined with gradient echo's sensitivity to local

15222586, 2004, 2, Downloaded from https://onlinelibrary.wiley.com/doi/10.1002/jmri.10451 by Cochrane Chile, Wiley Online Library on [17/08/2023]. See the Terms and Conditions (https://onlinelibrary.wiley.com/terms-and-conditions) on Wiley Online Library for rules of use; OA articles are governed by the applicable Creative Commons License

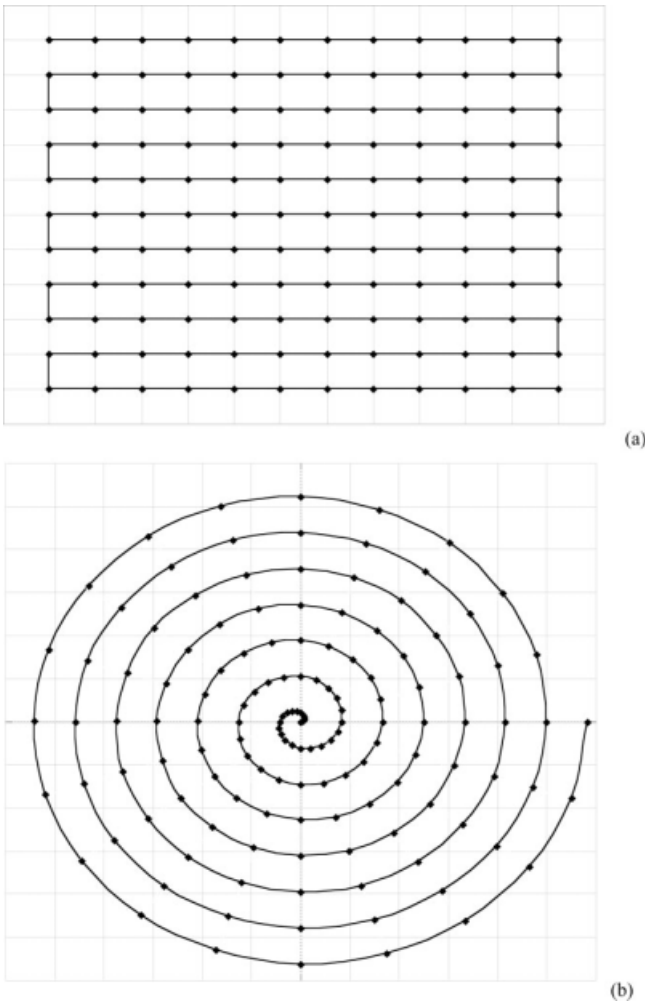

Figure 7. K-space trajectories for blipped EPI (**a**), spiral imaging (**b**, solid line), and radial imaging (**b**, dashed lines). In both EPI and spiral imaging, essentially all of the k-space can be traversed in one execution of the pulse sequence, although multishot versions using interleaved trajectories are often used for purposes of maintaining a certain TE for T2 or T2* contrast. Note that for the blipped EPI trajectory (a), the data points, indicated by small diamonds, are uniformly spaced on a grid providing equal weight to low- and high-spatial-frequency data and facilitating image reconstruction via the two-dimensional FT. Note that the spiral and radial trajectories (b) heavily sample the center of k-space where the low-spatial-frequency data, encoding general shape and contrast, is mapped. In this particular spiral example, the collected points lie on radial lines (dashed lines), which facilitates usage of a projection reconstruction technique for image reconstruction. Alternatively, the points can be interpolated to create a grid of points that can be reconstructed with an FT.

changes in oxygenation (the BOLD, or blood oxygen level-dependent effect (26–29)), makes gradient echo EPI very useful for functional MRI (fMRI) studies of brain function. However, while the total scan time is much shorter for EPI than for non-EPI scans, the actual data acquisition time per excitation for EPI is longer since all of k-space is sampled rather than just one line. High-speed gradient systems allow for rapid traversal of the k_x axis, but traversal of the k_y axis is slow relative to the signal decay constant T2* and relative to the time it takes for chemical shift, magnetic susceptibility, and other field distortion artifacts (16,17,19,30) to evolve to an easily noticed level. Recalling THP 5, these artifacts are seen in the y or phase encoding direction of EPI scans since the k_y axis is the axis of k-space that is traversed most slowly. Indeed, the accumulation of chemical shift effects can result in fat and water images displaced from each other by many pixels, requiring the use of fat saturation pulses (31–34) or spectrally selective excitation (35,36) to obtain an interpretable view of the water (wet tissue) image. Magnetic susceptibility and field distortion artifacts will apply to all tissues and result in local stretching and shrinking of the image and signal dropout that can be quite severe (17,18).

Assuming roughly 10 or more seconds have passed since the last scan, repetition time (TR) is effectively infinite for a single-shot EP image. An infinite TR is an attractive feature in that it allows collection of scans with contrast completely independent of T1. When EP images are acquired at intervals on the order of one to two seconds, as might be the case for an fMRI (27,37,38) series, TR is not effectively infinite and both T1 and T2 (spin echo EPI) or T1 and T2* (gradient echo EPI) influence contrast.

Hybrid Trajectories

There are a number of techniques that involve acquisition of more than one line of k-space per excitation but less than the entire k-space matrix. Often in a spin echo sequence, two 180° refocusing RF pulses are applied in each excitation, with a spin echo collected after each 180°. These echoes can be reconstructed as separate proton density and T2 images, each with a unique and consistent TE. However, the data from two or more different echoes, when appropriately phase encoded, can instead be combined in one k-space array and reconstructed as one image with mixed contrast. Such a scan is called fast spin echo (FSE) (39,40), turbo spin echo (TSE) (41), or rapid-acquisition relaxation-enhanced (RARE) (42), with the number of echoes from one excitation that are combined into one image called the echo train length. Obviously, the scan time is reduced in this case by a factor equivalent to the echo train length. A consequence of these FSE/TSE/RARE sequences with their multiple 180° refocusing pulses is the deposition of large amounts of power into the patient. As clinical practice expands to include higher magnetic fields of 3.0 T and above, power deposition increases and motivates the use of sequences using RF refocusing pulses less than 180°, with a lower specific absorption ratio (SAR) deposition. Such incomplete refocusing pulses increase the complexity of the signal, yet the magnetization can be recovered through the use of hyperechoes—echoes of echoes—that recover signal while allowing faster scanning with less power deposition (43). Multishot EPI is another low-power hybrid technique with many, but not all, of the lines of k-space acquired after one excitation. In this case, scan time is reduced compared to that for non-EPI rectilinear scans by the number of k-space lines acquired per shot.

15222586, 2004, 2, Downloaded from https://onlinelibrary.wiley.com/doi/10.1002/jmri.10451 by Cochrane Chile, Wiley Online Library on [17/08/2023]. See the Terms and Conditions (https://onlinelibrary.wiley.com/terms-and-conditions) on Wiley Online Library for rules of use; OA articles are governed by the applicable Creative Commons License

Radial Trajectories

A special property of k-space is that the data along any line passing through the origin of k-space represent the FT of the projection of the imaged tissue onto a line with the same orientation in image space (44,45). This is often called the central slice theorem (or the projection slice theorem or central section theorem) and is take-home point 6. As an example, let the image intensities from all the tissue in an imaged slice be projected onto the x axis (similar to a projection in computed tomography) and then FT that projection. The result is equal to the row of data at $k_y = 0$. Similarly, if the image intensities from all the tissue in an imaged slice are projected onto the y axis and that projected signal is Fourier transformed, the result is equal to the data column at $k_x = 0$. Armed with this principle, one can easily see that radial lines of k-space data (Fig. 7b) can be Fourier transformed to produce a set of radial projections. These projections can then be reconstructed into an image using any of the algorithms used to reconstruct CT images such as filtered back-projection or Fourier reconstruction (44,45). This is called projection reconstruction MRI.

One significant advantage of projection reconstruction MRI is that radial projections starting near the origin of k-space can be acquired right away after excitation (i.e., with extremely short TEs), allowing imaging of tissues with very short T2*s such as lung parenchyma (46,47). The short TEs are possible since, recalling THP 1, only short-duration gradient activity is needed to move a small amount away from the k-space origin. Another advantage of radial techniques is that the center of k-space is heavily sampled, which improves the image SNR (13,48,49).

Spiral Trajectories

Spiral acquisitions, like those for EPI, involve trajectories that sweep over k-space very rapidly, covering all or a large portion of k-space in one execution of the pulse sequence. However, unlike EPI, spiral trajectories typically either start (most commonly) or end at the origin of k-space and trace out a spiral path as shown in Fig. 7b. Spiral acquisitions can be single or multishot (50) with data from multiple shots interleaved to fill in gaps between the trajectories of individual shots. Spiral imaging offers the significant advantage over other k-space trajectories in that data collection is fairly symmetric about the center of k-space, meaning that the data in one circuit of a spiral passing near points $(+k_{x1}, +k_{y1})$, $(-k_{x1}, +k_{y1})$, $(-k_{x1}, -k_{y1})$, and $(+k_{x1}, -k_{y1})$ are all acquired in rapid succession over a narrow time window followed by collection of the next circuit of points near $(+k_{x2}, +k_{y2})$, $(-k_{x2}, +k_{y2})$, $(-k_{x2}, -k_{y2})$, and $(+k_{x2}, -k_{y2})$, and so on. This symmetry and early sampling of the center of k-space minimizes several otherwise significant artifacts such as those due to flow and motion (50,51). The disadvantage of spiral techniques is increased blurring (52–54). Depending on the specific spiral trajectory, the data either are reconstructed using the same techniques used for radial scans or are interpolated onto a grid and then Fourier transformed to create an image.

Incomplete Filling of K-Space

Often, either to shorten total scan time or to shorten echo time, k-space is only partially filled. If high-spatial-frequency data (that which is at the periphery of k-space) are omitted, then a lower-resolution image results (see Fig. 6a–c). To attempt to counter this effect, the missing high-spatial-frequency k-space data are often filled in with zeros (Fig. 5a). This is called zero-filling or zero-filling interpolation (ZIP) and has the effect in the image domain of interpolating the image along the spatial axis (e.g., x or y) corresponding to the k-space axis that was zero-filled (11,55). This is what happens when the acquisition matrix is, say, 192×256, but the reconstructed image is 256×256. Zero-filling can be used with any of the trajectories described in this paper. Although the interpolation accomplished by zero-filling may improve the appearance of the image, the truncation or omission of high-spatial-frequency data results in an artifact known as truncation artifact, ringing, or Gibbs ringing (see Fig. 5a) (11), and the collection of less than the full matrix of points results in lower SNR.

It is also possible to acquire slightly more than half of the k-space data, say all data for $k_y \geq 0$, and then to use the inherent symmetry of the data to create a reasonable estimate for the missing data before reconstructing the image. This is called half- or partial-Fourier imaging (56,57). Note that while these techniques save time, the acquisition of less than a complete data set reduces the image SNR and details are not as crisp as they would be if the entire k-space data set were acquired.

MOTION

Motion presents unique challenges and opportunities in MRI. To avoid blurring and ghosting (58,59), k-space must be filled in a such a way that there is little to no difference in the position of every tissue in the slice when each data point is acquired. One way to do this is to acquire the entire data set in a time that is very short relative to the motion, such as an ultrafast gradient echo scan (e.g., 128 k_y lines * 2-msec TR = 256-msec acquisition time) of a liver moving over a 10,000-msec long respiratory cycle. Another option, of course, is to attempt to eliminate the motion, for example, through breath holding or immobilization.

Data acquisition can be synchronized with cyclic motions such as cardiac contraction or respiration. This is the basis of cine MRI for cardiovascular applications. Through prospective or retrospective triggering (60), data are only written to any given k-space array when the moving object (e.g., the heart) returns to the same position. The time window over which data for one image are collected within one motion cycle is kept small enough that effectively no motion occurs. Note that for the sake of reducing total scan time, segmented scans acquire a segment of k-space (i.e., several lines) using multiple excitations within one motion cycle (61). In this case, the time window over which data for one image are collected within one motion cycle is lengthened, which introduces blurring and potentially other artifacts depending on changes that may occur while collecting a segment of k-space or between segments.

15222586, 2004, 2, Downloaded from https://onlinelibrary.wiley.com/doi/10.1002/jmri.10451 by Cochrane Chile, Wiley Online Library on [17/08/2023]. See the Terms and Conditions (https://onlinelibrary.wiley.com/terms-and-conditions) on Wiley Online Library for rules of use; OA articles are governed by the applicable Creative Commons License

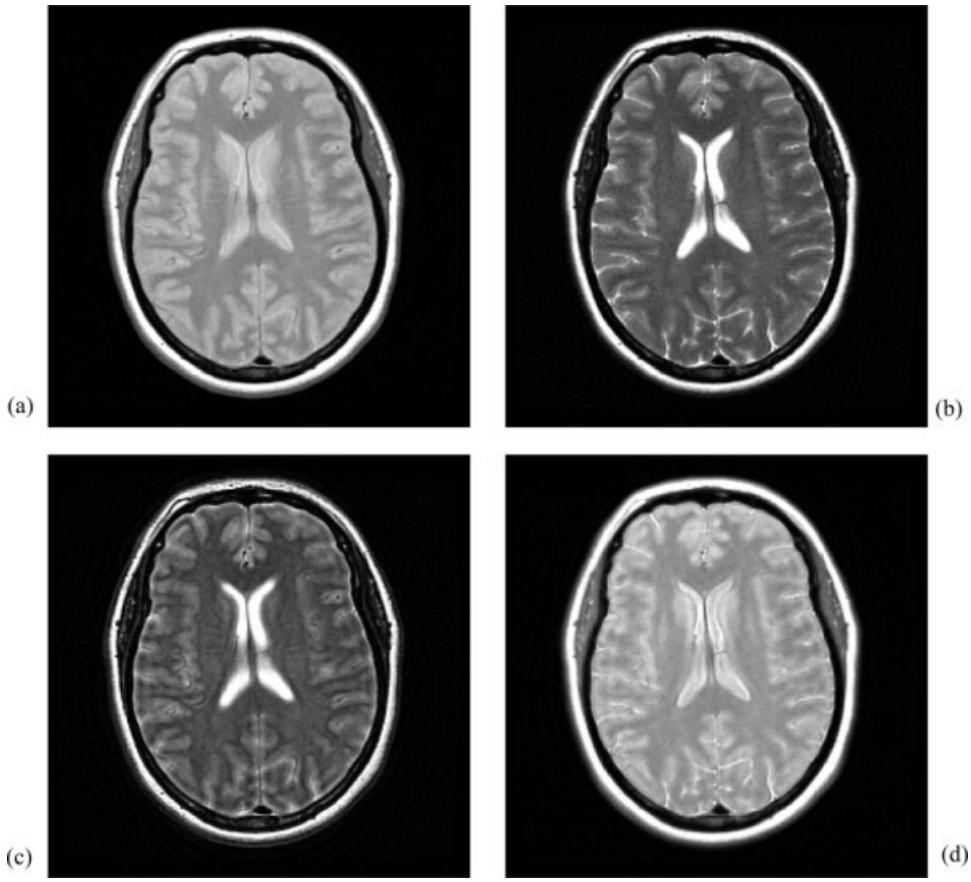

Figure 8. Proton density (**a**)- and T2 (**b**)-weighted spin echo axial brain images, each reconstructed from a 256 × 256 k-space array. To illustrate the point that most image information, including contrast and general shape, is contained in the low-spatial-frequency data in the center of k-space (THP 4), the central 32 × 32 points of the proton density k-space data was replaced with that from the T2 image and an image reconstructed (**c**). Note that while less than 7% of the data came from the T2 data, the image looks much more like the T2 image (b) than the proton density image (a). When the central 32 × 32 points of the T2 k-space data are replaced by those from the proton density k-space array, the reconstructed image (**d**) looks most like the proton density image (a); however, some high-spatial-frequency details like the appearance of bright cerebrospinal fluid (CSF) in the sulci matches the T2-weighted high-spatial-frequency information from which the image was reconstructed.

EFFECT OF TRAJECTORY ON IMAGES

If the relative contrast between different tissues does not change over the course of the scan (i.e., the magnetization is in steady state), then the k-space trajectory will have no influence on image contrast. However, if relative contrast between different tissues does change over the course of the scan, then the trajectory will have a dramatic effect on image contrast. The relative contrast extant when the central portion of k-space is filled will dominate the image contrast (recall THP 4), as shown in Fig. 8.

There are several situations in which relative contrast changes over the course of a scan. These include passage of a bolus of contrast agent, recovery after a preparatory RF pulse such as an inversion pulse or a fat saturation pulse, lack of a steady state, generation of hyperechoes (43), T2* decay (especially relevant to EPI and spiral scans), and inflow of unsaturated blood. It is important to time the filling of central k-space so that the desired image contrast is obtained. For example, one might use a delay between injection of contrast agent and acquisition of the central k-space data to produce an image with appearance dominated by the effects of the peak contrast agent concentration (62,63). In addition to a delay, in non-EPI rectilinear scanning, changing the acquisition order of k-space lines from sequential to centric (starting at the center and working outward) or even to reverse centric (starting at the periphery and working inward) can be used to adjust the filling of k-space so that each portion is filled at the most optimal time. Similarly, spiral trajectories can start at the center of k-space and spiral out or start at the periphery and spiral inward (64) with different effects on the image.

In addition to the variable effects on image contrast brought on by the interplay between k-space trajectory and changes in relative contrast over the course of image acquisition, there is another effect—filtering. At the most basic level, filtering results in image blurring. This effect can be reduced by strategies such as reordering schemes (65–67) and inverse filtering (67) that minimize the effects of changes in relative contrast and tissue position occurring over the course of filling k-space. These strategies are not always advisable though, since they may conflict with other imaging priorities. With the exception of the T2*-dependent blurring seen in single-shot EPI and spiral scans, this filtering effect is often subtle and may for the most part be ignored. A textual and graphical explanation of filtering for imaging is given in an article by Hansen (68); mathematical and graphical explanations of filtering can be found in nearly any signals and systems textbook (e.g., 11).

K-SPACE TEMPORAL MANIPULATION

Not only can the order of k-space filling be manipulated to affect contrast, but variations in k-space filling can also be used to increase imaging speed. One method for this can be called view sharing, which is used to create

15222586, 2004, 2, Downloaded from https://onlinelibrary.wiley.com/doi/10.1002/jmri.10451 by Cochrane Chile, Wiley Online Library on [17/08/2023]. See the Terms and Conditions (https://onlinelibrary.wiley.com/terms-and-conditions) on Wiley Online Library for rules of use; OA articles are governed by the applicable Creative Commons License

a sliding window reconstruction of the image as it is being formed (69). This technique gives more frequent updates of the lower-spatial-frequency (i.e., central) lines of k-space but shares the higher-spatial-frequency (i.e., peripheral) lines of k-space. The image formed has the advantage of updating the contrast-forming central lines of k-space twice as fast as the edge-forming peripheral lines of k-space by repeating a (beginning-central-end-central) k-space collection scheme. Two similar sequential k-space manipulation methods, keyhole (63,70,71) and generalized series reconstruction (72,73), also use very rapid updates to the center of k-space, but with very slow or nonvarying updates to the peripheral areas of k-space. These methods are advantageous in applications involving rapidly changing contrast such as first-pass contrast bolus imaging, spin tagging, perfusion imaging, and diffusion imaging protocols but that do not have rapid changes in edge information for structures in the image.

An expansion on such methods is UNFOLD (unaliasing by Fourier-encoding the overlaps using the temporal dimension), which uses frame-to-frame variations in an undersampled k-space to produce images that vary in the imaging sequence (74). This holds promise for a software advancement of imaging capabilities for applications that require increased temporal resolution and varying temporal signatures of functions of interest. The initial applications of this technique are in imaging cardiac function.

PARALLEL IMAGING TECHNIQUES

One of the more promising recent developments in MRI methods is the introduction of parallel imaging techniques such as SMASH (simultaneous acquisition of spatial harmonics) (75) and SENSE (sensitivity encoding) (76). In these techniques, the unique position from which each tissue signal arises is encoded both by traditional gradient (k-space) encoding, as described earlier, and by the simultaneous use of multiple receiver coils, as in a phased array coil, as illustrated in Fig. 9a, c, and d.

Recalling the musical analogy used earlier, the statement was made that, ignoring the spectral richness of the human voice and the stereo nature of auditory perception, it would not be possible for a listener at a distance to determine the location of the loudest singer in a chorus of altos singing in unison. However, multiple listeners located close to the chorus would be able to distinguish differences in loudness. These multiple receivers—listeners analogous to the multiple receiver coils of a phased array coil—detect spatial encoding information that is complementary to that provided by having the choristers sing with different phases and keys. This is take-home point 7: multiple receiver coils operated in parallel can be used to acquire spatial encoding information that is complementary to that provided by traditional gradient (k-space) encoding.

The additional encoding afforded by the multiple receiver coils allows a reduction in the number of k-space lines acquired, with the reduction determined by the acceleration factor, which in current implementations can range from 1.5–4 for most applications. An acceleration factor of 2 requires the use of at least two coils and allows the number of k-space lines acquired to be reduced by a factor of 2. In this case, every other line of a full k-space matrix is acquired using traditional gradient encoding. If just these lines were reconstructed into an image, a very aliased image would result (see Fig. 9f and g) given that Δk_y was effectively doubled, thus halving the field of view (see Fig. 4). If the acceleration factor were 4, every fourth line would be acquired, using four or more receiver coils. Parallel imaging techniques then use numerical methods to in effect synthesize the otherwise uncollected image data and reconstruct an unaliased image.

SMASH (75) and SENSE (76) are currently the most prevalent parallel imaging techniques. Though both techniques utilize the position of the receiver coils with respect to the patient for signal encoding, SMASH directly generates the missing k-space lines prior to the FFT used to reconstruct the final image. SENSE uses the receiver coil sensitivity profiles (as in Fig. 9b) to perform a similar operation in image space after the undersampled data recorded by each coil are reconstructed into an aliased image (Fig. 9f and g). Simulated images showing different aspects of these techniques are presented in Fig. 9. Madore and Pelc (77) published a comparison of SMASH and SENSE along with another parallel imaging method.

The reduced scan time in parallel imaging comes at the price of two factors. The first is the SNR of the image, which is reduced at a minimum by the square root of the acceleration factor. Thus, a scan with an acceleration factor of 2 requires half the imaging time for the same resolution but with $(1/\sqrt{2})$ or 70.7% the SNR. Thus, an image series can be acquired more rapidly with the resulting images having degraded SNR. The other cost is an artifact in the image, which is related to the numerical operations for the acceleration. This artifact comes from the orientation of the scan plane relative to the geometry of the receiver coils. Most applications endeavor to minimize this artifact by optimizing coil geometry for the required scan plane. Current clinical and research applications that can profit from these techniques mainly require many repeated images of the same plane with a premium being placed on temporal resolution of the image data. Some examples include cardiac imaging (78), diffusion imaging for stroke (79), functional imaging (80), and interventional methods requiring high temporal resolution.

ARTIFACTS

Understanding k-space basics makes it easier to determine the source of artifacts in MR images, although a firm grasp of the FT is important too. For example, artifacts that are large in feature size such as broad stripes or a moiré pattern are typically encoded in the middle of k-space (recall THP 2), while artifacts that are fine in feature size such as narrow stripes or ringing arise from the periphery of k-space. Artifacts in MRI are well reviewed in a number of other publications (81–85).

15222586, 2004, 2, Downloaded from https://onlinelibrary.wiley.com/doi/10.1002/jmri.10451 by Cochrane Chile, Wiley Online Library on [17/08/2023]. See the Terms and Conditions (https://onlinelibrary.wiley.com/terms-and-conditions) on Wiley Online Library for rules of use; OA articles are governed by the applicable Creative Commons License

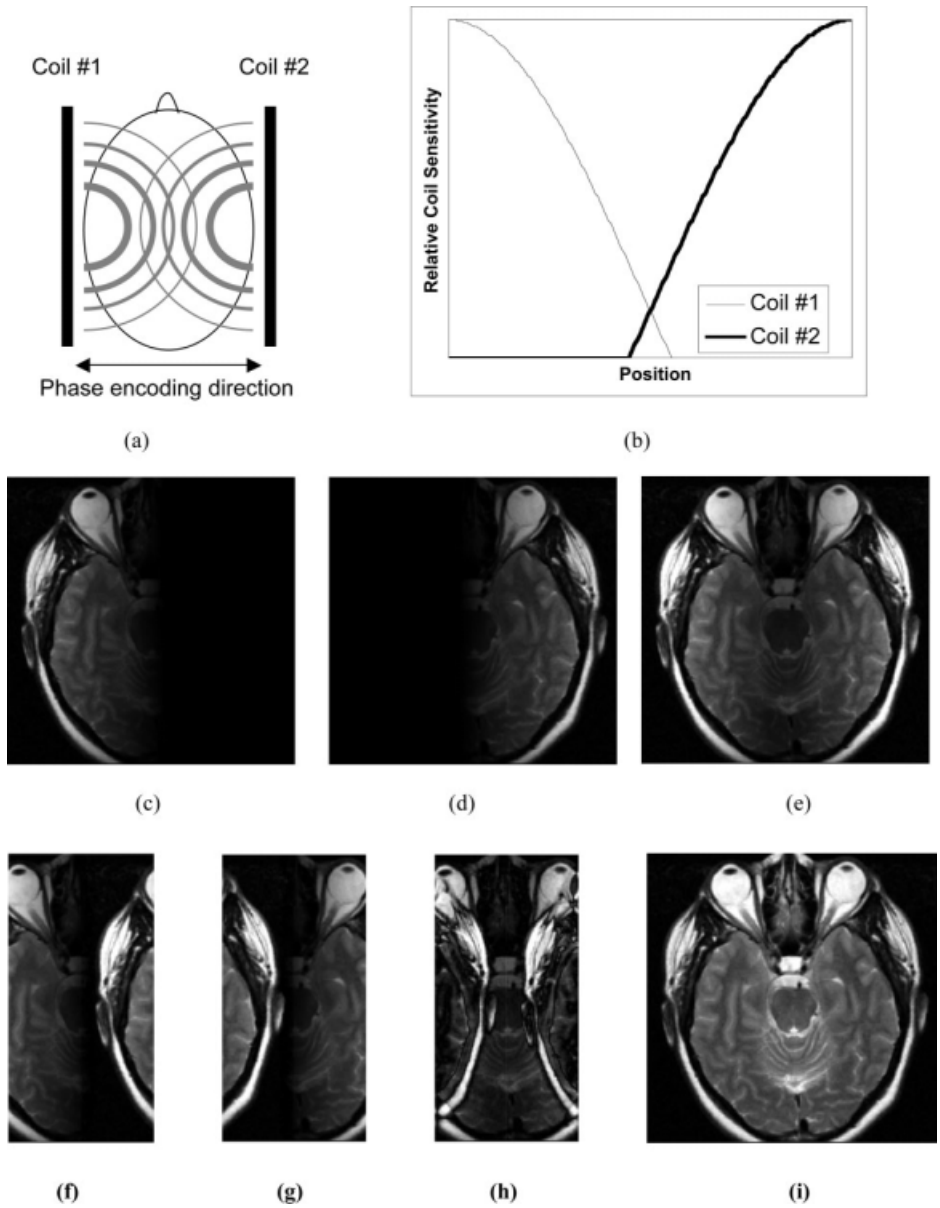

Figure 9. Simulated images illustrating parallel imaging techniques of SMASH and SENSE. Suppose two receiver coils are placed on either side of the head (**a**) with each coil having an axial sensitivity as shown in panel **b**. Assume that axial images with phase encoding along the right-left axis are acquired. With full k-space encoding, an image reconstructed using only data from coil 1 would appear as in panel **c**, while coil 2 would produce image **d**, each illustrating the respective coil's spatial sensitivity. A sum of squares combination of the full k-space data from both coils produces image **e**, with an obvious central vertical band of low signal. If instead of filling the entire k-space matrix every other k-space line is acquired, Δk_y is doubled and thus the field of view in the phase encoding direction is halved. Consequently, serious aliasing is seen in the new images from coils 1 (**f**) and 2 (**g**) and both coils in simple combination (**h**). If, instead of simply combining the undersampled k-space data from both coils, the missing k-space lines are generated prior to the FFT as in the SMASH method, then an unaliased image can be reconstructed, similar to that in panel **i**. Alternatively, the SENSE method uses the receiver coil sensitivity profiles (as in panel b) to perform a similar operation after the FFT, combining image data from panels f and e to produce an image like that in panel i.

SUMMARY

Many pulse sequence variations depend not on changes in the RF pulses applied but in the many different gradient magnetic field manipulations and coil arrangements used to map the collected data into k-space. Take-home points about k-space identified in this article, summarized here, relate the characteristics of the gradient waveforms to the k-space trajectory and the k-space data to the final image.

1. The net strength and duration of the gradient events govern how far and in what direction from the origin of k-space ($k_x = 0$, $k_y = 0$) a data point belongs.
2. Low-amplitude and/or short-duration gradient events encode low-spatial-frequency information; these data are mapped to the center of k-space. Conversely, high-amplitude and/or long-duration gradient events encode high-spatial-frequency information; this information is mapped to the periphery of k-space.
3. The farther the data collection extends from the origin of k-space, the better the nominal spatial resolution of the image.
4. Most image information, including contrast and general shape, is contained in the low-spatial-frequency data mapped to the center of k-space.
5. Chemical shift, magnetic susceptibility, and other field distortion artifacts, typically seen as distortions and blurring, are most readily seen across the image space dimension corresponding to the k-space axis that was most slowly traversed.
6. The data along any line passing through the origin of k-space represent the FT of the projection of the imaged tissue onto a line with the same orientation in image space.
7. Multiple receiver coils operated in parallel can be used to acquire spatial encoding information that

15222586, 2004, 2, Downloaded from https://onlinelibrary.wiley.com/doi/10.1002/jmri.10451 by Cochrane Chile, Wiley Online Library on [17/08/2023]. See the Terms and Conditions (https://onlinelibrary.wiley.com/terms-and-conditions) on Wiley Online Library for rules of use; OA articles are governed by the applicable Creative Commons License

is complementary to that provided by traditional gradient (k-space) encoding.

Having now an understanding of k-space, the reader is prepared to digest much of the research in MRI and to make well-informed decisions about clinical protocols. Keeping in mind the take-home points from this article, the impacts of choices in clinical protocols on the spatial, temporal, and contrast resolution of the resulting images are more easily understood.

REFERENCES

1. Hennig J. K-space sampling strategies. Eur Radiol 1999;9:1020–1031.
2. Mezrich R. A perspective on k-space. Radiology 1995;195:297–315.
3. Duerk JL. Principles of MR image formation and reconstruction. Magn Reson Imaging Clin N Am 1999;7:629–659.
4. Elster AD, Burdette JH. Questions & answers in magnetic resonance imaging. 2nd edition. St. Louis, MO: Mosby; 2001. p 79–105.
5. Brown M, Semelka RC, editors. MRI: basic principles and applications. 2nd edition. New York: Wiley-Liss; 2003. p 27–35.
6. Liang Z-P, Lauterbur PC. Principles of magnetic resonance imaging: a signal processing perspective. Piscataway, NJ: Wiley IEEE Press; 2000. p 141–172.
7. Haacke EM, Brown RW, Thompson MR, Venkatesan R. Magnetic resonance imaging: physical principles and sequence design. New York: John Wiley & Sons; 1999. p 165–204.
8. Mitchell DG. MRI principles. Philadelphia: W.B. Saunders; 1999. p 39–55.
9. Bushberg JT, Seibert JA, Leidholdt Jr EM, Boone JM. The essential physics of medical imaging. 2nd edition. Baltimore: Williams & Wilkins Publishers; 2001. p 415–430.
10. Brigham EO. The fast Fourier transform. Englewood Cliffs, NJ: Prentice-Hall; 1974. p 75–109.
11. Oppenheim AV, Willsky AS, Nawab SH. Signals and systems. 2nd edition. Englewood Cliffs, NJ: Prentice-Hall; 1996. p 515.
12. Bronskill MJ, McVeigh ER, Kucharczyk W, Henkelman RM. Syrinx-like artifacts on MR images of the spinal cord. Radiology 1988;166:485–488.
13. Forbes KP, Pipe JG, Bird CR, Heiserman JE. PROPELLER MRI: clinical testing of a novel technique for quantification and compensation of head motion. J Magn Reson Imaging 2001;14:215–222.
14. Lufkin R, Anselmo M, Crues J, Smoker W, Hanafee W. Magnetic field strength dependence of chemical shift artifacts. Comput Med Imaging Graphics 1988;12:89–96.
15. Smith RC, Lange RC, McCarthy SM. Chemical shift artifact: dependence on shape and orientation of the lipid-water interface. Radiology 1991;181:225–229.
16. Ludeke KM, Roschmann P, Tischler R. Susceptibility artifacts in NMR imaging. Magn Reson Imaging 1985;3:329–343.
17. Schmithorst VJ, Bernard JD, Holland SK. Simultaneous correction of ghost and geometric distortion artifacts in EPI using a multiecho reference scan. IEEE Trans Med Imaging 2001;20:535–539.
18. Ojemann JG, Akdubak E, Snyder AZ, McKinstry RC, Raichle ME. Anatomic localization and quantitative analysis of gradient refocused echo-planar fMRI susceptibility artifacts. Neuroimage 1997;6:156–167.
19. Chang H, Fitzpatrick JM. A technique for accurate magnetic-resonance-imaging in the presence of field inhomogeneities. IEEE Trans Med Imaging 1992;11:319–329.
20. Mitchell DG, Ortega H, Mohamed F, Tascyian T, Vinitski S. Aortic ghost artifact in ultrashort TE multislice gradient echo MR images is not increased by paramagnetic enhancement. Magn Reson Med 1993;29:269–272.
21. Frank LR, Buxton RB, Kerber CW. Pulsatile flow artifacts in 3D magnetic resonance imaging. Magn Reson Med 1993;30:296–304.
22. Runge VM, Wood ML. Fast imaging and other motion artifact reduction schemes: a pictorial overview. Magn Reson Imaging 1988;6:595–607.
23. Colletti PM, Raval JK, Benson RC, et al. The motion artifact suppression technique (MAST) in magnetic resonance imaging: clinical results. Magn Reson Imaging 1988;6:293–299.
24. Reese TG, Pearlman JD. MR gradient response modeling to ensure excitation coherence. J Magn Reson Imaging 1994;4:569–576.
25. Harvey PR, Mansfield P. Resonant trapezoidal gradient generation for use in echo-planar imaging. Magn Reson Imaging 1994;12:93–100.
26. Ogawa S, Menon RS, Tank DW, et al. Functional brain mapping by blood oxygenation level-dependent contrast magnetic resonance imaging. A comparison of signal characteristics with a biophysical model. Biophys J 1993;64:803–812.
27. Howseman AM, Bowtell RW. Functional magnetic resonance imaging: imaging techniques and contrast mechanisms. Philos Trans R Soc Lond B Biol Sci 1999;354:1179–1194.
28. Forster BB, MacKay AL, Whittall KP, et al. Functional magnetic resonance imaging: the basics of blood-oxygen-level dependent (BOLD) imaging. Can Assoc Radiol J 1998;49:320–329.
29. Turner R. Signal sources in bold contrast fMRI. Adv Exp Med Biol 1997;413:19–25.
30. Chen NK, Wyrwicz AM. Correction for EPI distortions using multi-echo gradient-echo imaging. Magn Reson Med 1999;41:1206–1213.
31. Trattnig S, Huber M, Breitenseher MJ, et al. Imaging articular cartilage defects with 3D fat-suppressed echo planar imaging: comparison with conventional 3D fat-suppressed gradient echo sequence and correlation with histology. J Comput Assist Tomogr 1998;22:8–14.
32. Wielopolski PA, Manning WJ, Edelman RR. Single breath-hold volumetric imaging of the heart using magnetization-prepared 3-dimensional segmented echo planar imaging. J Magn Reson Imaging 1995;5:403–409.
33. Reimer P, Ladebeck R, Rummeny EJ, et al. Initial feasibility studies using single-shot EPI for the detection of focal liver lesions. Magn Reson Med 1994;32:733–737.
34. Ba-Ssalamah A, Schibany N, Puig S, Herneth AM, Noebauer-Huhmann IM, Trattnig S. Imaging articular cartilage defects in the ankle joint with 3D fat-suppressed echo planar imaging: comparison with conventional 3D fat-suppressed gradient echo imaging. J Magn Reson Imaging 2002;16:209–216.
35. Block W, Pauly J, Kerr A, Nishimura D. Consistent fat suppression with compensated spectral-spatial pulses. Magn Reson Med 1997;38:198–206.
36. Schick F, Forster J, Machann J, Kuntz R, Claussen CD. Improved clinical echo-planar MRI using spatial-spectral excitation. J Magn Reson Imaging 1998;8:960–967.
37. Cohen MS. Real-time functional magnetic resonance imaging. Methods 2001;25:201–220.
38. Turner R, Howseman A, Rees GE, Josephs O, Friston K. Functional magnetic resonance imaging of the human brain: data acquisition and analysis. Exp Brain Res 1998;123:5–12.
39. Listerud J, Einstein S, Outwater E, Kressel HY. First principles of fast spin echo. Magn Reson Q 1992;8:199–244.
40. Constable RT, Anderson AW, Zhong J, Gore JC. Factors influencing contrast in fast spin-echo MR imaging. Magn Reson Imaging 1992;10:497–511.
41. Seelos KC, von Smekal A, Vahlensieck M, Gieseke J, Reiser M. Cardiac abnormalities: assessment with T2-weighted turbo spin-echo MR imaging with electrocardiogram gating at 0.5 T. Radiology 1993;189:517–522.
42. Hennig J, Nauerth A, Friedburg H. RARE imaging: a fast imaging method for clinical MR. Magn Reson Med 1986;3:823–833.
43. Hennig J, Scheffler K. Hyperechoes. Magn Reson Med 2001;46:6–12.
44. Brooks RA, Di Chiro G. Theory of image reconstruction in computed tomography. Radiology 1975;117:561–572.
45. Brooks RA, Di Chiro G. Principles of computer assisted tomography (CAT) in radiographic and radioisotopic imaging. Phys Med Biol 1976;21:689–732.
46. Bergin CJ, Pauly JM, Macovski A. Lung parenchyma: projection reconstruction MR imaging. Radiology 1991;179:777–781.
47. Bergin CJ, Noll DC, Pauly JM, Glover GH, Macovski A. MR imaging of lung parenchyma: a solution to susceptibility. Radiology 1992;183:673–676.
48. Pipe JG. Reconstructing MR images from undersampled data: data-weighting considerations. Magn Reson Med 2000;43:867–875.
49. Lauzon ML, Rutt BK. Polar sampling in k-space: reconstruction effects. Magn Reson Med 1998;40:769–782.
50. Meyer CH, Hu BS, Nishimura DG, Macovski A. Fast spiral coronary artery imaging. Magn Reson Med 1992;28:202–213.
51. Glover GH, Lee AT. Motion artifacts in fMRI: comparison of 2DFT with PR and spiral scan methods. Magn Reson Med 1995;33:624–635.

15222586, 2004, 2, Downloaded from https://onlinelibrary.wiley.com/doi/10.1002/jmri.10451 by Cochrane Chile, Wiley Online Library on [17/08/2023]. See the Terms and Conditions (https://onlinelibrary.wiley.com/terms-and-conditions) on Wiley Online Library for rules of use; OA articles are governed by the applicable Creative Commons License

52. Man LC, Pauly JM, Macovski A. Improved automatic off-resonance correction without a field map in spiral imaging. Magn Reson Med 1997;37:906–913.
53. King KF, Foo TK, Crawford CR. Optimized gradient waveforms for spiral scanning. Magn Reson Med 1995;34:156–160.
54. Pfeuffer J, Van de Moortele PF, Ugurbil K, Hu X, Glover GH. Correction of physiologically induced global off-resonance effects in dynamic echo-planar and spiral functional imaging. Magn Reson Med 2002;47:344–353.
55. Bernstein MA, Fain SB, Riederer SJ. Effect of windowing and zero-filled reconstruction of MRI data on spatial resolution and acquisition strategy. J Magn Reson Imaging 2001;14:270–280.
56. Feinberg DA, Hale JD, Watts JC, Kaufman L, Mark A. Halving MR imaging time by conjugation: demonstration at 3.5 kG. Radiology 1986;161:527–531.
57. Perman WH, el-Ghazzawy O, Gado MH, Larson KB, Perlmutter JS. A half-Fourier gradient echo technique for dynamic MR imaging. Magn Reson Imaging 1993;11:357–366.
58. Runge VM, Wood ML. Fast imaging and other motion artifact reduction schemes: a pictorial overview. Magn Reson Imaging 1988; 6:595–607.
59. Mitchell DG. Abdominal magnetic resonance imaging: optimization and artifact suppression. Top Magn Reson Imaging 1992;4:18–34.
60. Lenz GW, Haacke EM, White RD. Retrospective cardiac gating: a review of technical aspects and future directions. Magn Reson Imaging 1989;7:445–455.
61. Edelman RR, Wallner B, Singer A, Atkinson DJ, Saini S. Segmented TurboFLASH: method for breath-hold MR imaging of the liver with flexible contrast. Radiology 1990;177:515–521.
62. Kanematsu M, Shiratori Y, Hoshi H, Kondo H, Matsuo M, Moriwaki H. Pancreas and peripancratic vessels: effect of imaging delay on gadolinium enhancement at dynamic gradient recalled-echo MR imaging. Radiology 2000;215:95–102.
63. Chenevert TL, Helvie MA, Aisen AM, et al. Dynamic three-dimensional imaging with partial k-space sampling: initial application for gadolinium-enhanced rate characterization of breast lesions. Radiology 1995;196:135–142.
64. Glover GH, Law CS. Spiral-in/out BOLD fMRI for increased SNR and reduced susceptibility artifacts. Magn Reson Med 2001;46: 515–522.
65. Bailes DR, Gilderdale DJ, Bydder GM, Collins AG, Firmin DN. Respiratory ordered phase encoding (ROPE): a method for reducing respiratory motion artifacts in MR imaging. J Comput Assist Tomogr 1985;9:835–838.
66. Butts K, Riederer SJ, Ehman RL. The effect of respiration on the contrast and sharpness of liver lesions in MRI. Magn Reson Med 1995;33:1–7.
67. Deichmann R, Good CD, Josephs O, Ashburner J, Turner R. Optimization of 3-D MP-RAGE sequences for structural brain imaging. Neuroimage 2000;12:112–127.
68. Hansen CL. Digital image processing for clinicians, part II: filtering. J Nucl Cardiol 2002;9:429–437.
69. Foo TK, Bernstein MA, Aisen AM, Hernandez DJ, Colleck BD, Bernstein T. Improved ejection fraction and flow velocity estimates with use of view sharing and uniform repetition time excitation with fast cardiac techniques. Radiology 1995;195:471–478.
70. van Vaals JJ, Brummer ME, Dixon WT, et al. "Keyhole" method for accelerating imaging of contrast agent uptake. J Magn Reson Imaging 1993;3:671–675.
71. Jones RA, Haraldseth O, Muller TB, Rinck PA, Oksendal AN. K-space substitution: a novel dynamic imaging technique. Magn Reson Med 1993;29:830–834.
72. Webb AG, Liang ZP, Magin RL, Lauterbur PC. Applications of reduced-encoding MR imaging with generalized-series reconstruction (RIGR). J Magn Reson Imaging 1993;3:925–928.
73. Chandra S, Liang ZP, Webb A, Lee H, Morris HD, Lauterbur PC. Application of reduced-encoding imaging with generalized-series reconstruction (RIGR) in dynamic MR imaging. J Magn Reson Imaging 1996;6:783–797.
74. Madore B, Glover GH, Pelc NJ. Unaliasing by Fourier-encoding the overlaps using the temporal dimension (UNFOLD) applied to cardiac imaging and fMRI. Magn Reson Med 1999;42:813–828.
75. Sodickson DK, Manning WJ. Simultaneous acquisition of spatial harmonics (SMASH): fast imaging with radiofrequency coil arrays. Magn Reson Med 1997;38:591–603.
76. Pruessmann KP, Weiger M, Scheidegger MB, Boesiger P. SENSE: sensitvity encoding for fast MRI. Magn Reson Med 1999;42:952–962.
77. Madore B, Pelc NJ. SMASH and SENSE: experimental and numerical comparisons. Magn Reson Med 2001;45:1103–1111.
78. Pruessmann KP, Wiger M, Boesiger P. Sensitivity encoded cardiac MRI. J Cardiovasc Magn Reson 2001;3:1–9.
79. Bammer R, Keeling SL, Augustin M, et al. Improved diffusion-weighted single-shot echo-planar imaging (EPI) in stroke using sensitivity encoding (SENSE). Magn Reson Med 2001;46:548–554.
80. Golay X, Pruessman KP, Weiger M, et al. PRESTO-SENSE: an ultrafast whole-brain fMRI technique. Magn Reson Med 2000;43: 779–786.
81. Henkelman RM, Bronskill MJ. Artifacts in magnetic resonance imaging. Rev Magn Reson Med 1987;2:1–126.
82. Wood ML, Henkelman RM. Artifacts. In: Stark DD, Bradley Jr WG, editors. Magnetic resonance imaging. 3rd edition, volume 1. St. Louis, MO: Mosby, Inc.; 1999. Chapter 10.
83. Hinks RS, Quencer RM. Motion artifacts in brain and spine MR. Radiol Clin N Am 1988;26:737–753.
84. Mirowitz SA. MR imaging artifacts: challenges and solutions. Magn Reson Imaging Clin N Am 1999;7:717–732.
85. Hood MN, Ho VB, Smirniotopoulos JG, Szumowski J. Chemical shift: the artifact and clinical tool revisited. Radiographics 1999; 19:357–371.

15222586, 2004, 2, Downloaded from https://onlinelibrary.wiley.com/doi/10.1002/jmri.10451 by Cochrane Chile, Wiley Online Library on [17/08/2023]. See the Terms and Conditions (https://onlinelibrary.wiley.com/terms-and-conditions) on Wiley Online Library for rules of use; OA articles are governed by the applicable Creative Commons License